

Selective C–H Activation Facilitated by the Cooperative Effect of Extrinsic O₂ and Na on Ag(111)

Zhaoyu Zhang, Rujia Hou, Chi Zhang,* and Wei Xu*

Cite This: *ACS Catal.* 2025, 15, 12085–12093

Read Online

ACCESS |



Metrics & More



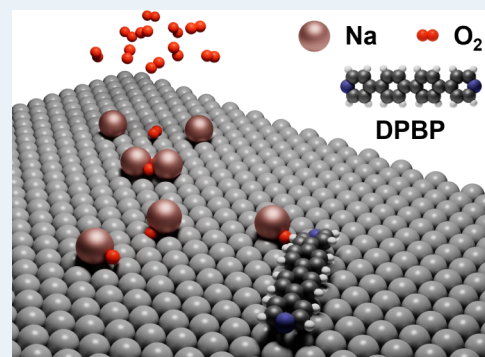
Article Recommendations



Supporting Information

ABSTRACT: Carbon–hydrogen (C–H) bond activation is pivotal in chemistry. On-surface C–H activation reactions, generally identified as endothermic processes, have been extensively explored via the modification of molecule–substrate systems. In addition, extrinsic components (e.g., O₂) have been introduced to circumvent high energy barriers and steer reaction selectivity. Specifically, oxygen exhibits unique catalytic behavior in enabling C(sp²)–H activation on Ag(111) in an exothermic way. However, the chemical inertness and low sticking probability of Ag(111) toward O₂ prohibit its efficient utilization on the pristine surface. In this study, through the combination of scanning tunneling microscopy (STM) imaging and density functional theory (DFT) calculations, we report an on-surface synthesis strategy for the efficient C(sp²)–H activation of pyridyl groups on Ag(111) via the cooperative effect of extrinsic O₂ and Na. The synergistic interplay between O₂ and Na has also been systematically elucidated. These results would be inspiring not only for harnessing the oxidative potential of O₂ in C–H activation processes but also for enriching the toolkit for on-surface synthesis.

KEYWORDS: on-surface chemistry, on-surface reaction, C–H activation, scanning tunneling microscopy, density functional theory



INTRODUCTION

C–H bonds, representing the most ubiquitous yet relatively inert chemical linkages in organic frameworks, are highly valued for their pivotal role in self- or cross-coupling reactions, particularly for the construction of π -conjugated organic architectures.^{1–3} Building upon these intrinsic reactivities, transition metals provide a versatile catalytic platform for precise C–H bond activation, enabling stereochemical control and enhancing reaction efficiency unattainable through classical approaches.⁴ In this regard, atomically flat transition-metal surfaces (e.g., Au, Ag, Cu) not only serve as model systems of catalysts with crystallographically well-defined structures for on-surface reactions,^{5,6} but also provide ideal two-dimensional platforms for the characterization of nanostructures.^{7,8} Crucially, while a wide range of on-surface C–H activation reactions have been reported under ultrahigh vacuum (UHV) conditions,^{9–12} they are generally identified as endothermic processes and the rate-limiting step in the coupling reaction cascades. To facilitate C–H activation, concerted research efforts have been devoted to the engineering of molecule–substrate interfaces, including variation of substrate types and orientations,^{13–16} rational design of molecular precursors,^{17–19} and more.

Moreover, the introduction of extrinsic components into on-surface molecular reactions has proven to be promising in circumventing these high energy barriers and steering reaction selectivity.^{20–26} Among others, oxygen, as an oxidative agent,

has shown remarkable efficacy in regulating C–H activation.²⁶ For example, it activates the C–H bonds in terminal alkynyl groups on Ag(111) and Au(111), facilitating the formation of extended organometallic C(sp)–M–C(sp) (M: metal) structures.^{27–30} In addition, it promotes the C–H activation within poly(para-phenylene) on Cu(111) by greatly lowering the reaction temperature.³¹ In particular, theoretical calculations indicate that both oxygen species, i.e., molecular O₂ and atomic O, are highly reactive upon adsorption on Ag(111),^{28,32,33} catalyzing such C–H activation in an exothermic manner, reversely. However, the chemical inertness and low sticking probability of Ag(111) toward O₂³⁴ make it challenging to efficiently utilize O₂ to facilitate the activation of some relatively stable C–H bonds on the pristine surface. Thus, this underscores the paramount importance of developing catalytic strategies to harness the oxidative potential of O₂ in C–H activation processes.

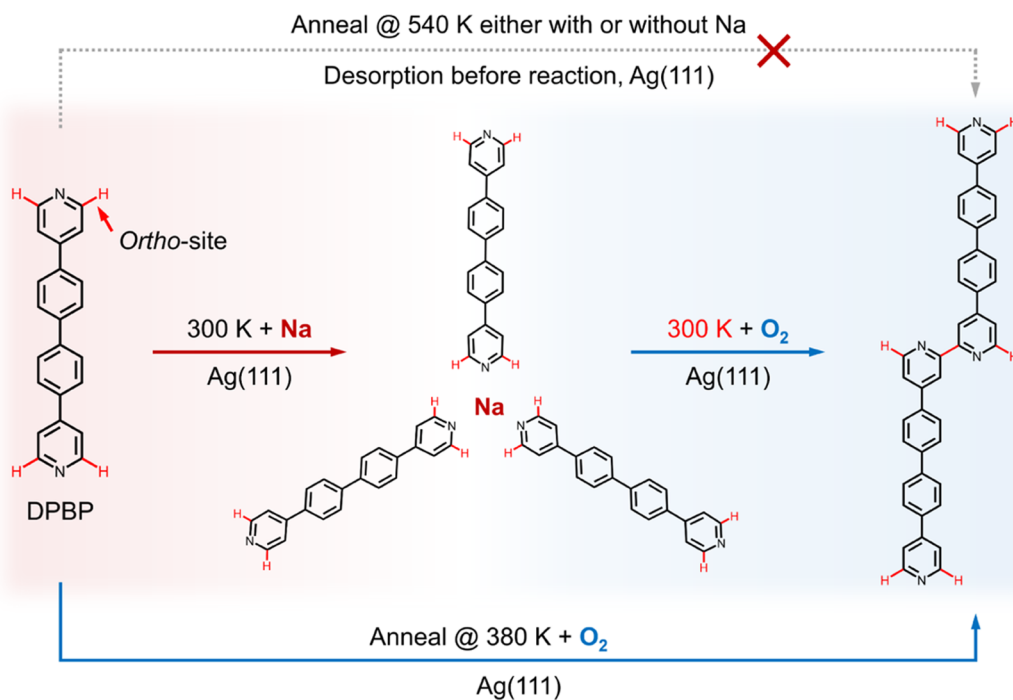
Herein, a strategy for the oxidative C–H activation of pyridyl groups (C(sp²)) on Ag(111) was developed based on the cooperative effect of extrinsic O₂ and Na, resulting in

Received: June 19, 2025

Revised: June 25, 2025

Accepted: June 26, 2025

Scheme 1. Selective C–H Activation and Coupling Reaction of DPBP Molecules on Ag(111) at 300 K (Onset Temperature) Facilitated by the Cooperative Effect of Na and O₂, which Is Inaccessible in the Absence of Either Na or O₂



efficient dehydrogenative coupling at room temperature (RT, ~ 300 K). Inspired by the K-promoted O₂ adsorption on Au(111)^{35,36} and the alkali metal-promoted reaction activity and selectivity in catalytic processes,^{37,38} the alkali metal Na was introduced onto Ag(111) to enhance O₂ adsorption in this study. The molecular precursor, 4,4'-di(pyridin-4-yl)-1,1'-biphenyl (abbreviated as DPBP, cf. Scheme 1), was selected to construct the model system, where both pyridine groups act as anchoring sites to interact with Na atoms.^{39–41} Intriguingly, direct thermal treatment of the DPBP-precovered Ag(111) sample at 540 K exclusively induced molecular desorption prior to reaction initiation, with Na incorporation failing to alter this phenomenon (indicated by the gray dotted arrows at the top of Scheme 1). In sharp contrast, annealing the same system under an O₂ atmosphere enabled dehydrogenative coupling at 380 K via selective C–H activation at the *ortho*-sites (blue arrow, bottom). Remarkably, the addition of Na to the DPBP-precovered Ag(111) sample at 300 K initiated the structural transformation (red arrow), with atomically dispersed Na located at the nodes of the resulting network. Subsequent exposure to O₂ triggered the *ortho*-site C–H activation and coupling reactions at 300 K (blue arrow, middle). By a combination of STM imaging and DFT calculations, we systematically elucidated the reaction processes and confirmed the synergistic interplay between extrinsic O₂ and Na in driving the C–H activation on Ag(111). In addition, the metadynamics calculations and transition-state search revealed that the Na nodes enhanced the adsorption and dissociation of O₂ on Ag(111), thereby enabling the oxygen-catalyzed selective C–H activation at RT. Our combined experimental and theoretical approach unraveled the indispensable dual role of Na and O₂ in facilitating the C(sp²)–H activation on Ag(111). This strategy, developed in the model system, should be beneficial for the activation of other robust C–H bonds while advancing the fundamental

understanding of alkali metal promotion effects in heterogeneous catalysis.

RESULTS AND DISCUSSION

Deposition of DPBP molecules on Ag(111) held at ~ 300 K yielded a well-ordered windmill-like network structure (Figure 1a). The close-up STM image (Figure 1b) resolved the rod-like single-molecule morphology within windmill-like four-molecule units. The DFT-optimized network structure (Figure 1c) and the corresponding simulated STM topography (the gray part) were further superimposed on the STM image (Figure 1b) with good agreement. In the structural model, the terminal N atoms engage adjacent molecules via C–H \cdots N hydrogen bonds, consistent with previous works.^{42,43} Such a hydrogen-bonding configuration further stabilizes the extended periodic network. Despite these intermolecular interactions, DPBP molecules failed to withstand thermal treatment and desorbed drastically at ~ 540 K (as indicated in Scheme 1) prior to any reactions.

Subsequently, Na atoms were dosed onto the DPBP-precovered sample (Figure 1a) held at ~ 300 K, resulting in a structural transformation to the honeycomb-like network (Figure 1d). The close-up STM image (Figure 1e) shows the dim feature at each junction of the network, consistent with a single Na center interacting with three neighboring DPBP molecules via electrostatic interactions.^{40,44} The DFT-optimized coassembled structural model of Na and DPBP (Figure 1f) further corroborates this scenario, showing an excellent match with the experimental observations in both structural periodicity and STM topography, as shown in Figure 1e. Notably, subsequent annealing at 540 K also induced the complete desorption of DPBP molecules without any evidence of reactions at this temperature or lower.

It has been verified that oxygen enables the efficient C(sp)–H activation of terminal alkynes on Ag(111) at RT and even

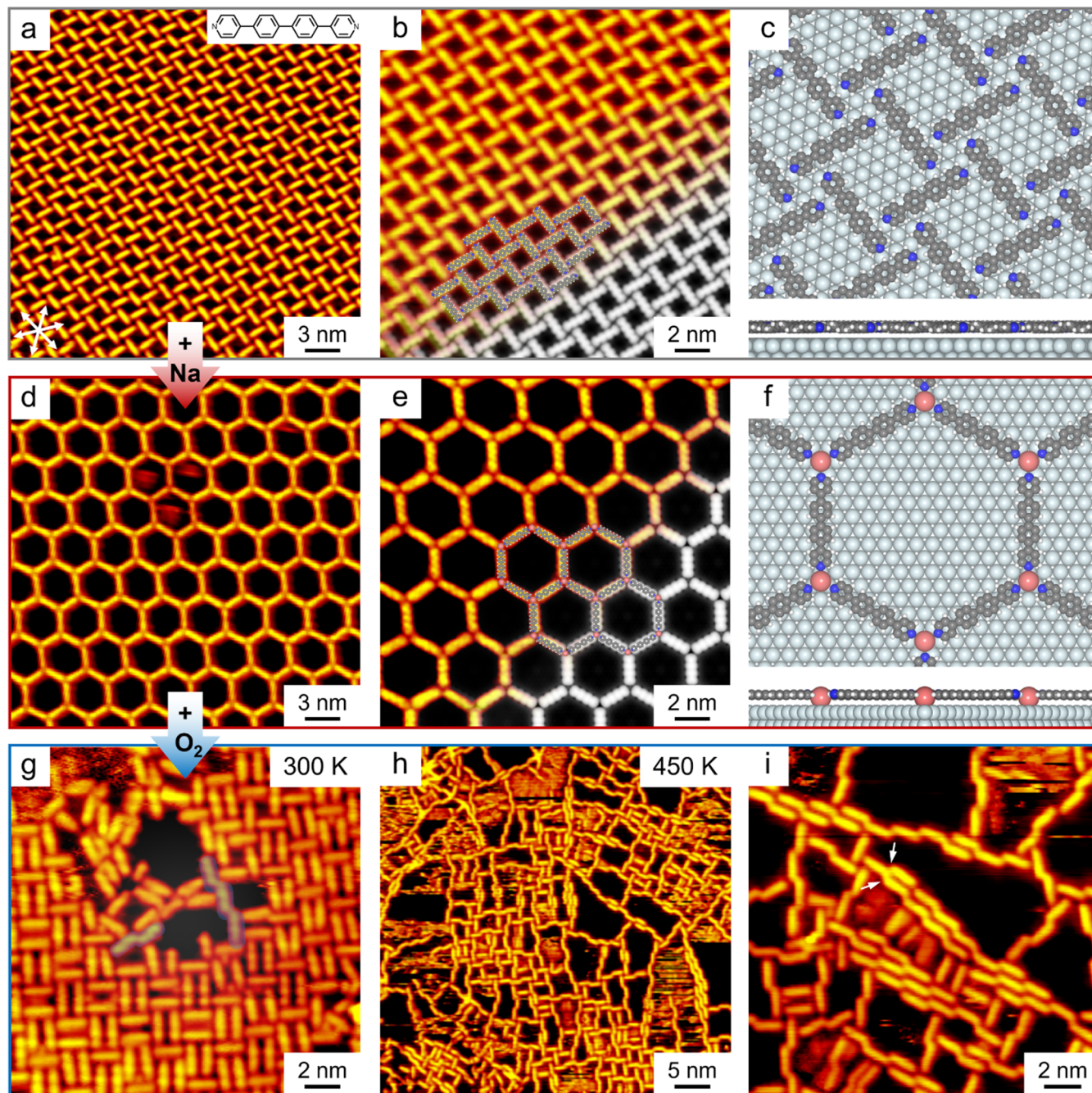


Figure 1. Dehydrogenative coupling reaction of DPBP molecules on Ag(111) promoted in the presence of both Na and O₂. (a) Large-scale and (b) close-up STM images of windmill-like DPBP structures obtained after deposition at 300 K, overlaid with the DFT-optimized structure and the corresponding STM simulation (gray part). (c) Top and side views of the DFT-optimized windmill-like network on Ag(111). (d,e) STM images of honeycomb-like coassembled structure obtained by dosing Na onto the above sample at 300 K, superimposed by the DFT-optimized network and the corresponding STM simulation (gray part). (f) DFT-optimized honeycomb-like network on Ag(111). C, gray; H, white; N, navy blue; Na, pink; Ag substrate, light blue. (g,h) STM images showing the dehydrogenative coupling reaction of DPBP molecules in the presence of Na, i.e., starting from the honeycomb-like network structure in (d), with further O₂ exposure while annealing the individual samples at (g) 300 and (h) 450 K, respectively. (i) Close-up STM image showing the formation of DPBP-based chains after annealing the honeycomb-like network at 450 K under an O₂ atmosphere. Scanning conditions: $V = 0.7$ V, and $I = 0.6$ nA.

lower^{27,28,30} by significantly reducing the reaction barriers and converting the process from endothermic to exothermic and thus directs the reaction pathway. Accordingly, O₂ was introduced into this molecular system as a potential catalyst to promote C(sp²)-H activation of pyridyl groups. Surprisingly, after exposing the honeycomb-like structure (Figure 1d) to the O₂ atmosphere at a pressure of $\sim 2 \times 10^{-7}$ mbar for 20

min (180 L) with the sample held at 300 K, covalent oligomers appeared (as shaded blue in Figure 1g), and the Na-incorporated network was entirely disrupted. Due to the low density of states of Na, the Na-based species cannot be identified from STM images. Notably, after O₂ exposure to a similar honeycomb-like coassembled sample at $\sim 1 \times 10^{-7}$ mbar for 20 min (90 L) while annealing at 450 K, the structure

was completely destroyed with the formation of long staggered chains (Figure 1h). The zoomed-in STM image (Figure 1i) provides more details on the DPBP molecular units predominantly connected together in a shoulder-to-shoulder alignment, forming dimers, oligomers, and chains. In addition, U-shaped bifurcated structures were also observable, as indicated by the white arrows, suggesting that more sites were activated, followed by coupling reactions.

To further distinguish the role of Na in the reactions, the DPBP-precovered Ag(111) sample (Figure 2a) was then

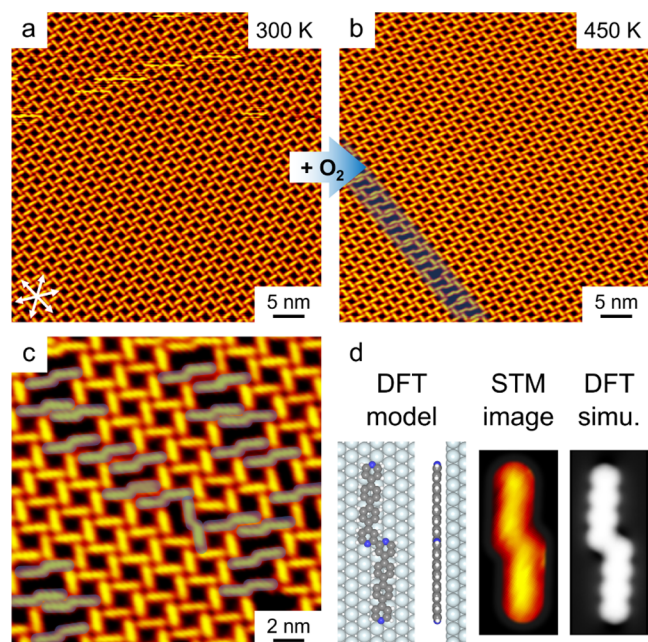


Figure 2. Dehydrogenative coupling reaction of DPBP molecules on Ag(111) promoted by O₂ exclusively. (a,b) Large-scale STM images showing (a) DPBP assembled windmill-like structure and (b) the appearance of dimers (shaded blue) after annealing at 450 K under O₂ atmosphere. (c) Close-up STM image showing the formation of DPBP-based dimers (shaded blue). (d) Magnified STM image, simulated STM topography, and DFT-optimized model of a DPBP-coupled dimer on Ag(111). C, gray; H, white; N, navy blue; Ag substrate, light blue. Scanning conditions: $V = 0.7$ V and $I = 0.6$ nA.

exposed to an O₂ atmosphere during thermal treatment in the absence of Na. Interestingly, exposing such a sample to O₂ (360 L) while annealing at ~ 380 K led to the appearance of several DPBP-based dimers (Figure S1a,b), indicating the onset temperature. Specifically, by annealing the sample at higher temperatures (~ 450 K) during the exposure of the sample to O₂ (90 L), long rows of dimers (shaded blue) were found to be distributed on the sample and embedded in the windmill-like network of intact DPBP molecules (Figure 2b), in direct contrast to the Na-involved situation with the same dosage (Figure 1h,i). Moreover, Figure S1 also exhibits distinct coupling efficiency in Na-free versus Na-modified systems under identical conditions (380 K, O₂ atmosphere), revealing the critical role of Na in enhancing the reaction kinetics.

From the magnified STM image (Figure 2c), the detailed morphology of dimers can be identified, as indicated by the blue silhouettes. In these dimer structures, two neighboring molecular units are uniformly connected in the same shoulder-to-shoulder manner. This structural configuration aligns with the C–C coupling characteristics resulting from *ortho*-site C–

H activation, as previously reported.⁴⁵ Based on the consistency of the covalent connections formed in these cases, DFT calculations were further performed on the structure simplified as a dimer. Note that within the pyridine groups, the C–H bonds are generally destabilized at the *ortho*-site due to the existence of N sites, allowing for the selective C–H activation.¹⁸ Based on the characteristics of the connection and the similarity in the morphology to the previous works,^{14,45} the dimer structure was optimized with C–C coupling at the *ortho*-sites as shown in Figure 2d (right). The corresponding STM simulation (right) nicely reproduced the experimental one (middle) in both topography and dimensions, thus confirming the structural assignment.

It is also worth noting that thermal treatment of either the DPBP self-assembled structure or the DPBP and Na coassembled structure failed to trigger any reaction before desorption, indicating that the incorporation of Na alone did not affect the reaction process. On the contrary, when O₂ was introduced, the reaction temperature of C–H activation was greatly reduced and became feasible before desorption. More interestingly, the integration of both Na and O₂ successfully facilitated the reaction at even lower temperatures (300 K). These phenomena suggest that O₂ alone catalyzes the C–H activation with a low efficiency, while the interplay between Na and O₂ serves as cocatalysts, dramatically facilitating the C–H activation performance with much higher efficiency.

It has been well established that the interaction between O₂ and Ag(111) is generally very weak, and the probability of dissociation is very low, especially at ~ 300 K.³⁴ Meanwhile, theoretical calculations predict that alkali metals adsorbed on Ag(111) can enhance the adsorption and dissociation of O₂ in the ethylene or propylene epoxidation,^{46,47} serving as a promoter. To further understand the role of Na in the dramatic enhancement of the O₂-assisted reaction performance in our system, it should be crucial to investigate the configurations of O₂ molecules in the presence or absence of Na on Ag(111). In addition, the experimental temperature (i.e., 300 K) is an important parameter for C–H activation that should be taken into consideration. Accordingly, the metadynamics method within the framework of *ab initio* molecular dynamics (AIMD) (see Methods for more details) was employed, with the reaction temperature set to 300 K, to systematically search the reaction pathways of O₂ adsorbed on Ag(111) without and with the incorporation of Na atoms, respectively. The two-dimensional free energy surfaces for both cases are illustrated in Figure 3, depicting the bond length between the two oxygen atoms as a function of the coordination number. The coordination number quantifies the binding degree of the two oxygens to the adjacent Ag or Na atoms, with higher values corresponding to more interacting surface atoms and thus stronger binding interactions.

As shown in Figure 3a, initially, two oxygen atoms are in their most stable adsorption state (IS_1) with the lowest free energy of -1.08 eV and the O–O bond length of 1.40 Å, indicating its chemisorption.³⁴ As the coordination number decreases, the length of the O–O bond shortens with a desorption tendency (indicated by the white dashed arrow). The corresponding structure (I_1) exhibits a free energy of -0.21 eV. The desorption barrier for O₂ on Ag(111) is determined to be 1.02 eV, which is in agreement with a previous report⁴⁸ and allows its occurrence at 300 K.⁴⁹ This

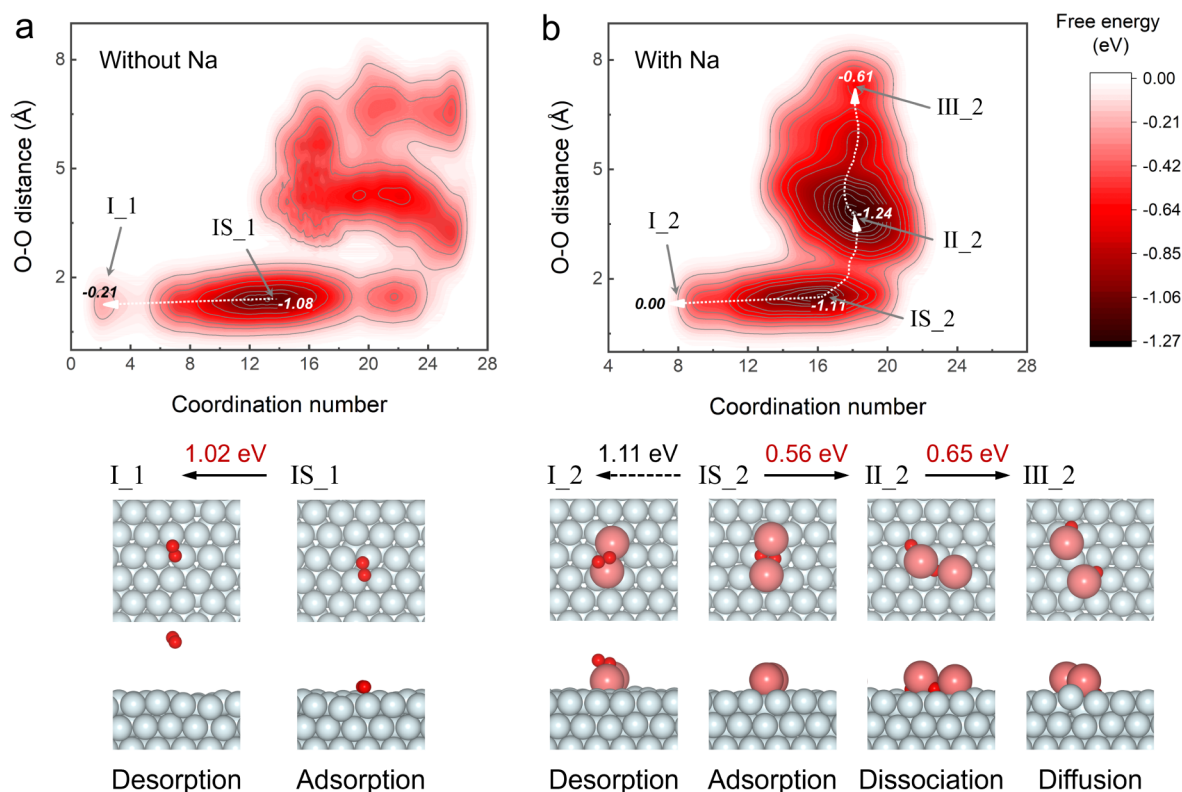


Figure 3. Two-dimensional free energy surfaces of an oxygen molecule adsorbed on Ag(111) at 300 K (a) without and (b) with the incorporation of Na atoms, illustrating the O–O bond length as a function of the coordination number. The coordination number represents the average number of Ag or Na atoms adjacent to the two oxygen atoms within a defined spatial cutoff, as determined by their interatomic distances. Points IS, I, II, and III denote the locations of initial states and local energy minima along the reaction pathways, respectively, with their corresponding structures displayed at the bottom. The scale of the contour maps (right) indicates free energy changes in eV relative to the highest-energy reference states within the respective systems, and the energy values for the specific structures are also marked. Na, pink; O, red; Ag substrate, light blue.

result is also consistent with the low sticking probability of Ag(111) toward O_2 ³⁴.

When Na is present on Ag(111), the situation totally changed (Figure 3b). Previous reports experimentally show that K atoms on Au(111) enhanced the adsorption of O_2 , forming K_xO_y species,^{35,36} and DFT calculations suggest the formation of K_2O_2 structure. In our case, a similar Na_2O_2 configuration was adopted and further confirmed as a stable chemisorption state (IS_2) by AIMD simulations, with a free energy of -1.11 eV. Surprisingly, with the assistance of Na, the Na_2O_2 structure evolves into the globally most stable configuration II_2, with a free energy of -1.24 eV, on the 2D free energy surface. This structure is characterized by a higher coordination number and an extended O–O distance (3.75 Å), suggesting that Na promotes oxygen adsorption on Ag(111) in a dissociated form after oxygen fixation. The energy barrier from the Na-assisted chemisorbed state (IS_2) to the dissociated state (II_2) was calculated to be 0.56 eV. In addition, the desorption pathway was not explicitly found in the computational analysis due to the persistent Na-mediated interactions, with only partial detachment of the two oxygen atoms from Ag(111). This indicates that complete O_2 desorption necessitates overcoming Na-induced stabilization, requiring an activation barrier exceeding 1.11 eV. Critically, the dissociation (IS_2 \rightarrow II_2) barrier remains significantly lower than that of the competing desorption pathway (IS_2 \rightarrow I_2 \rightarrow further desorption), highlighting the kinetically favored dissociation pathway in the presence of Na. Interestingly, the dissociation is followed by a potential diffusion process toward

III_2 (-0.61 eV) with a reaction barrier of 0.65 eV. Therefore, the AIMD simulations imply that the presence of Na promotes the fixation and dissociation of oxygen on Ag(111), with this pathway being both kinetically and thermodynamically more favorable than the desorption pathway. In addition, further diffusion of the sodium oxides is possible at 300 K.

To elucidate the reaction mechanism of C–H activation and clarify the synergistic role of Na and O_2 in this process, transition-state search has been further conducted based on the climbing image-nudged elastic band (CI-NEB) method, considering four distinct conditions (left panel of Figure 4). When a single DPBP molecule is adsorbed on Ag(111), the corresponding C–H activation process (as depicted by gray dotted lines) is highly endothermic, with a prohibitively high reaction barrier of 2.30 eV, rendering the process kinetically inaccessible before molecular desorption. Similarly, in the presence of Na, although Na interacts with the N site on the pyridyl ring in the C–H activation process, the reaction remains strongly endothermic, with an energy barrier of 2.39 eV (gray solid lines). This is because Na tends to prevent the pyridyl ring from bending toward Ag(111), which inhibits the formation of surface-stabilized radicals and leads to an even higher energy barrier. Thus, the addition of Na exerts a negligible thermodynamic and kinetic influence on the reaction scenario, fully consistent with experimental results.

Building on this, the introduction of oxygen species was also investigated. To simplify the systems, the adsorption of O_2 and NaO is applied as model systems representing the O_2 atmosphere and sodium oxide Na_xO_y formation, respectively.

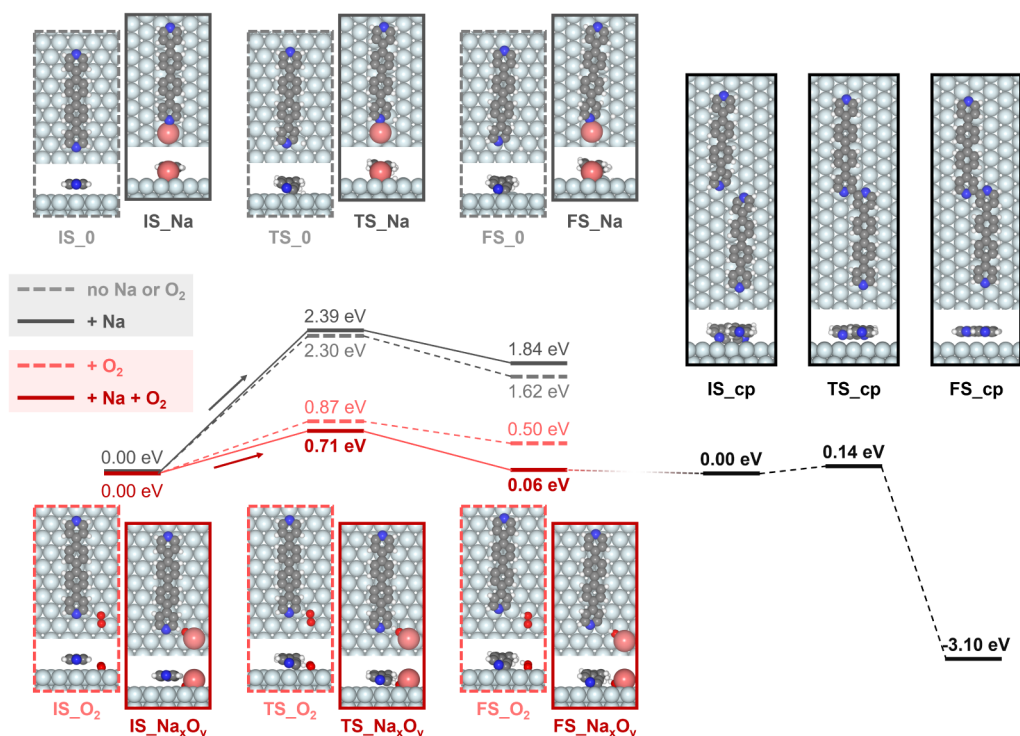


Figure 4. DFT-calculated reaction pathways for *ortho*-site C–H activation and the subsequent C–C coupling reaction of a DPBP molecule on Ag(111). Left panel: the C–H activation pathways under four distinct conditions: (i) absence of both Na and O₂ (gray dotted lines), (ii) presence of Na alone (gray solid lines), (iii) presence of O₂ alone (red dotted lines), and (iv) coexistence of both Na and O₂ (red solid lines). Right panel: the following C–C coupling pathway. The structural models of the initial states (IS), transition states (TS), and final states (FS) under each condition are displayed, with their relative energies referenced to their respective IS. C, gray; H, white; N, navy blue; Na, pink; O, red; Ag substrate, light blue.

Assuming the adsorption of O₂ molecules on Ag(111), O₂ interacts with the DPBP molecule via the C–H···O hydrogen bond,²⁸ which drastically lowers the C–H activation barrier to 0.87 eV (red dotted lines) and further stabilizes the dissociated H atom. This indicates the catalytic potential of adsorbed oxygen on Ag(111). Nevertheless, AIMD simulations reveal a pronounced tendency for O₂ desorption, severely limiting the reaction efficiency. To circumvent this limitation, we investigated the synergistic effect between Na and oxygen based on a simplified Na_xO_y model. The Na_xO_y species can interact with the DPBP molecule via the C–H···O hydrogen bond, which also effectively facilitates C–H activation. As a result, the reaction barrier is reduced to 0.71 eV, and more notably, the inclusion of Na further stabilizes the dissociated H atom, with the final state (FS_{Na_xO_y}) being almost comparable to the initial state (IS_{Na_xO_y}) in the total energy. Thus, the cooperative interplay between Na atoms and O₂ enables the corresponding C–H activation process to be favored both thermodynamically and kinetically over alternative situations. Moreover, the AIMD results suggest the feasibility of forming such sodium oxides at 300 K. Consequently, the cooperative catalytic scenario leads to the remarkably enhanced C–H activation compared to the Na-free situation.

Thereafter, the C–C coupling process of two dehydrogenated DPBP radicals was calculated on Ag(111) as shown in the right panel of Figure 4. This process is highly exothermic, with an exceedingly low energy barrier of 0.14 eV, indicating that the C–H activation process is the rate-limiting step. These results directly correlate with experimental observations that

the divergent reaction performances stem from the distinct mechanistic roles of Na and oxygen in C–H activation. Specifically, the performance enhancement arises from two synergistic effects: (i) Na-promoted stabilization and dissociation of oxygen species on Ag(111), and (ii) oxygen-facilitated C–H bond cleavage. This cooperative catalytic mechanism, jointly validated by STM experiments and DFT calculations, establishes the foundation for the observed catalytic superiority of the Na–O₂ system.

It is also noteworthy that, while oxygen serves as a prevalent oxidant in catalytic systems, its utilization usually presents significant research challenges due to activation difficulties and the intricate modulation requirements of its electronic structures to confer targeted catalytic activities.^{34,50} This limitation becomes particularly evident on Ag(111), where the low viscosity coefficient and inertness to oxygen activation^{51,52} was reported to hinder oxygen utilization. Herein, our approach leverages organic molecular anchoring to achieve atomic dispersion of extrinsic Na atoms on Ag(111), enabling subsequent oxygen stabilization and dissociation under O₂ exposure. The cooperative effect of extrinsic O₂ and Na further results in the efficient oxidative C(sp²)–H activation of pyridyl groups on Ag(111), and the high selectivity of the *ortho*-site C–H activation is achieved due to N functionalization. Such a strategy provides a possible regulatory method for the utilization of O₂ on surfaces with inherent activation resistance, while the revealed synergistic mechanism further provides a blueprint for efficient on-surface C–H bond activation by harnessing the oxidative potential of O₂.

CONCLUSIONS

In conclusion, this study demonstrates an on-surface synthesis strategy for efficient C(sp²)-H activation of pyridyl groups on Ag(111) through the cooperative effect of extrinsic O₂ and Na. The combination of STM experiments and DFT calculations reveals distinct thermal-response reaction performances. The DPBP-precovered Ag(111) samples exhibited exclusive molecular desorption during thermal treatment regardless of Na presence, whereas O₂ exposure initiated catalytic *ortho*-site C-H activation followed by coupling. Notably, preintroduced Na coassembled with DPBP molecules significantly enhanced reaction efficiency under O₂ exposure. Metadynamics simulations and transition-state calculations elucidate the cooperative mechanism in which Na stabilizes O₂ and promotes its dissociation, forming Na_xO_y on Ag(111), which further catalyzes C-H activation with a significantly decreased reaction barrier. This strategy developed in the model system demonstrates great potential for facilitating C-H activation on noble metal surfaces under oxidative conditions, offering solutions to overcome the low sticking probability of O₂ on inert surfaces and expanding the synthetic toolkit for on-surface synthesis.

METHODS

Experimental Details. The STM experiments were conducted in an UHV chamber equipped with an “Aarhus-type” variable-temperature STM from SPECS^{53,54} and maintained at a base pressure of 1 × 10⁻¹⁰ mbar. The Ag(111) substrate was prepared by repeated cycles of Ar⁺ ion sputtering and annealing at approximately 800 K. A home-built molecular evaporator was employed for the sample preparation. Following thorough degassing, DPBP molecules (purchased from Yanshen Technology Co., Ltd., Jilin Chinese Academy of Sciences, with a purity exceeding 97%) were deposited via thermal sublimation at ~473 K onto Ag(111) substrate held at ~300 K. High-purity oxygen molecules were introduced into the preparation chamber via a leak valve at a pressure of ~1.0–2.0 × 10⁻⁷ mbar for different durations. Pure sodium (Na, from SAES Getters) was dosed using a wire-type Na dispenser by conventional resistance heating after complete degassing. The Na dosage was calibrated by applying the same constant current (~6.0 A) for 40 s per cycle, with additional Na added by increasing the deposition cycles. After sample preparation, it was then transferred to the STM head within the UHV chamber for imaging. Typical scanning parameters were set to *V* = 0.8 V and *I* = 0.5–0.8 nA. All the STM images were acquired within a temperature range of 100–150 K and were subsequently smoothed to reduce noise.

Calculation Details. The calculations were conducted within the density functional theory (DFT) framework using the Vienna Ab Initio Simulation Package (VASP).^{55,56} The projector-augmented wave (PAW) method was employed to describe the ion-electron interactions.^{57,58} The Perdew–Burke–Ernzerhof (PBE) generalized gradient approximation (GGA) functional was used for exchange correlation,⁵⁹ with van der Waals interactions included based on Grimme’s DFT-D3 dispersion correction.⁶⁰ The atomic structures were relaxed using the conjugate gradient algorithm until forces on all unconstrained atoms were ≤ 0.03 eV/Å. A plane-wave basis set with an energy cutoff of 400 eV was utilized. Ag(111) substrates were modeled as three-layer slabs separated by ~15 Å vacuum region, with the bottom one layer fixed. STM

images were simulated using the Tersoff–Hamann method,⁶¹ approximating the tunneling current through the local density of states (LDOS). For the metadynamics calculations, the optimized structures were used to initialize the molecular dynamics simulations. The annealing process involved a gradual increase in temperature from 0 to 300 K. The NVT ensemble was employed, with temperature control achieved via the velocity rescaling method in conjunction with a Nosé–Hoover thermostat.^{62–64} The annealing process lasted for 3 ps, using a time step of 1 fs, with the temperature incremented every 20 steps. Following annealing, the systems were equilibrated for 20 ps using a time step of 2 fs (totaling 10,000 steps) at 300 K, employing a Nosé–Hoover thermostat within the NVT ensemble. The equilibrated states were then used as starting points for the metadynamics simulations. The O–O distance and coordination numbers were selected as two-dimensional collective variables (CVs) for the metadynamics simulations. The coordination numbers were defined as the number of Ag or Na atoms within a certain distance of the O atoms. Specifically, the coordination number between O and Ag atoms was defined using a cutoff distance of 7.0 Å, while that between O and Na atoms used a cutoff of 5.0 Å. These cutoff distances were set to extend the search range for interactions beyond the typical bonding distances. The systems were continuously sampled for ~40 ps using a time step of 1 fs (totaling ~40,000 steps) at 300 K. In addition, transition states were identified using the climbing image-nudged elastic band (CI-NEB)⁶⁵ method until the forces acting on the path typically converged to ≤ 0.03 eV/Å.

ASSOCIATED CONTENT

Supporting Information

The Supporting Information is available free of charge at <https://pubs.acs.org/doi/10.1021/acscatal.5c04254>.

O₂-induced dehydrogenative coupling reaction of DPBP molecules on Ag(111) in the absence and presence of Na assistance under identical thermal conditions (380 K, which is the reaction onset temperature under the Na-free condition)(PDF)

AUTHOR INFORMATION

Corresponding Authors

Chi Zhang – Interdisciplinary Materials Research Center, School of Materials Science and Engineering, Tongji University, Shanghai 201804, People’s Republic of China; orcid.org/0000-0002-2335-4579; Email: zhangchi11@tongji.edu.cn

Wei Xu – Interdisciplinary Materials Research Center, School of Materials Science and Engineering, Tongji University, Shanghai 201804, People’s Republic of China; orcid.org/0000-0003-0216-794X; Email: xuwei@tongji.edu.cn

Authors

Zhaoyu Zhang – Interdisciplinary Materials Research Center, School of Materials Science and Engineering, Tongji University, Shanghai 201804, People’s Republic of China

Rujia Hou – Interdisciplinary Materials Research Center, School of Materials Science and Engineering, Tongji University, Shanghai 201804, People’s Republic of China

Complete contact information is available at: <https://pubs.acs.org/doi/10.1021/acscatal.5c04254>

Author Contributions

The manuscript was written with contributions from all authors. All authors have approved the final version of the manuscript.

Notes

The authors declare no competing financial interest.

ACKNOWLEDGMENTS

The authors acknowledge financial support from the National Key R&D Program of China (2023YFE0101900, from the Ministry of Science and Technology of the People's Republic of China), the National Natural Science Foundation of China (Grant Nos. 22202153 and 22125203), and the Fundamental Research Funds for the Central Universities. This work also utilized computational resources of the Supercomputer HOKUSAI BigWaterfull 2 provided by RIKEN through the HPCI System Research Project (Project ID: hp240096).

REFERENCES

- (1) Yi, H.; Zhang, G.; Wang, H.; Huang, Z.; Wang, J.; Singh, A. K.; Lei, A. Recent Advances in Radical C–H Activation/Radical Cross-Coupling. *Chem. Rev.* **2017**, *117*, 9016–9085.
- (2) Segawa, Y.; Maekawa, T.; Itami, K. Synthesis of Extended π -Systems through C–H Activation. *Angew. Chem., Int. Ed.* **2015**, *54*, 66–81.
- (3) Funes-Ardoiz, I.; Maseras, F. Oxidative Coupling Mechanisms: Current State of Understanding. *ACS Catal.* **2018**, *8*, 1161–1172.
- (4) Gandeepan, P.; Müller, T.; Zell, D.; Cera, G.; Warratz, S.; Ackermann, L. 3d Transition Metals for C–H Activation. *Chem. Rev.* **2019**, *119*, 2192–2452.
- (5) Grill, L.; Hecht, S. Covalent On-Surface Polymerization. *Nat. Chem.* **2020**, *12*, 115–130.
- (6) Clair, S.; de Oteyza, D. G. Controlling a Chemical Coupling Reaction on a Surface: Tools and Strategies for On-Surface Synthesis. *Chem. Rev.* **2019**, *119*, 4717–4776.
- (7) Song, S.; Su, J.; Telychko, M.; Li, J.; Li, G.; Li, Y.; Su, C.; Wu, J.; Lu, J. On-Surface Synthesis of Graphene Nanostructures with π -Magnetism. *Chem. Soc. Rev.* **2021**, *50*, 3238–3262.
- (8) Zhang, C.; Yi, Z.; Xu, W. Scanning Probe Microscopy in Probing Low-Dimensional Carbon-Based Nanostructures and Nanomaterials. *Mater. Futures* **2022**, *1*, 032301.
- (9) Björk, J.; Sánchez-Sánchez, C.; Chen, Q.; Pignedoli, C. A.; Rosen, J.; Ruffieux, P.; Feng, X.; Narita, A.; Müllen, K.; Fasel, R. The Role of Metal Adatoms in a Surface-Assisted Cyclodehydrogenation Reaction on a Gold Surface. *Angew. Chem., Int. Ed.* **2022**, *61*, No. e202212354.
- (10) Björk, J. Thermodynamics of an Electrocyclic Ring-Closure Reaction on Au(111). *J. Phys. Chem. C* **2016**, *120*, 21716–21721.
- (11) Kinikar, A.; Di Giovannantonio, M.; Urgel, J. I.; Eimre, K.; Qiu, Z.; Gu, Y.; Jin, E.; Narita, A.; Wang, X.-Y.; Müllen, K.; Ruffieux, P.; Pignedoli, C. A.; Fasel, R. On-Surface Polyarylene Synthesis by Cycloaromatization of Isopropyl Substituents. *Nat. Synth.* **2022**, *1*, 289–296.
- (12) Cai, Z.; Pang, R.; Liu, M.; Qin, H.; Chen, S.; Zhong, J.; Zhong, D. Linear Alkane Polymerization on Au-Covered Ag(110) Surfaces. *J. Phys. Chem. C* **2018**, *122*, 24209–24214.
- (13) Zhong, D.; Franke, J. H.; Podiyanchari, S. K.; Blömker, T.; Zhang, H.; Kehr, G.; Erker, G.; Fuchs, H.; Chi, L. Linear Alkane Polymerization on a Gold Surface. *Science* **2011**, *334*, 213–216.
- (14) Sun, Q.; Zhang, C.; Kong, H.; Tan, Q.; Xu, W. On-Surface Aryl–Aryl Coupling Via Selective C–H Activation. *Chem. Commun.* **2014**, *50*, 11825–11828.
- (15) Chen, S.; Cai, Z.; Ou, Z.; Wang, Z.; Guo, D.; Zhong, D. Direct Aryl–Aryl Coupling of Pentacene on Au(110). *Phys. Chem. Chem. Phys.* **2021**, *23*, 22155–22159.
- (16) Cai, Z.; She, L.; Wu, L.; Zhong, D. On-Surface Synthesis of Linear Polyphenyl Wires Guided by Surface Steric Effect. *J. Phys. Chem. C* **2016**, *120*, 6619–6624.
- (17) Gao, Y.; Huang, L.; Cao, Y.; Richter, M.; Qi, J.; Zheng, Q.; Yang, H.; Ma, J.; Chang, X.; Fu, X.; et al. Selective Activation of Four Quasi-Equivalent C–H bonds Yields N-Doped Graphene Nanoribbons with Partial Corannulene Motifs. *Nat. Commun.* **2022**, *13* (1), 6146.
- (18) Matena, M.; Riehm, T.; Stöhr, M.; Jung, T. A.; Gade, L. H. Transforming Surface Coordination Polymers into Covalent Surface Polymers: Linked Polycondensed Aromatics through Oligomerization of N-Heterocyclic Carbene Intermediates. *Angew. Chem., Int. Ed.* **2008**, *47*, 2414–2417.
- (19) Kocić, N.; Liu, X.; Chen, S.; Decurtins, S.; Krejčí, O.; Jelínek, P.; Repp, J.; Liu, S.-X. Control of Reactivity and Regioselectivity for On-Surface Dehydrogenative Aryl–Aryl Bond Formation. *J. Am. Chem. Soc.* **2016**, *138*, 5585–5593.
- (20) Li, C.; Xu, Z.; Zhang, Y.; Li, J.; Xue, N.; Li, R.; Zhong, M.; Wu, T.; Wang, Y.; Li, N.; et al. Structure Transformation from Sierpiński Triangles to Chains Assisted by Gas Molecules. *Natl. Sci. Rev.* **2023**, *10*, nwad088.
- (21) Lowe, B.; Hellerstedt, J.; Matěj, A.; Mutombo, P.; Kumar, D.; Ondráček, M.; Jelínek, P.; Schiffrin, A. Selective Activation of Aromatic C–H Bonds Catalyzed by Single Gold Atoms at Room Temperature. *J. Am. Chem. Soc.* **2022**, *144*, 21389–21397.
- (22) Sánchez-Sánchez, C.; Martínez, J. I.; Ruiz Del Arbol, N.; Ruffieux, P.; Fasel, R.; López, M. F.; de Andres, P. L.; Martín-Gago, J. Á. On-Surface Hydrogen-Induced Covalent Coupling of Polycyclic Aromatic Hydrocarbons via a Superhydrogenated Intermediate. *J. Am. Chem. Soc.* **2019**, *141*, 3550–3557.
- (23) Zhang, Z.; Gao, Y.; Yi, Z.; Zhang, C.; Xu, W. Separation of Halogen Atoms by Sodium from Dehalogenative Reactions on a Au(111) Surface. *ACS Nano* **2024**, *18*, 9082–9091.
- (24) Berdonces-Layunta, A.; Lawrence, J.; Edalatmanesh, S.; Castro-Esteban, J.; Wang, T.; Mohammed, M. S. G.; Colazzo, L.; Peña, D.; Jelínek, P.; de Oteyza, D. G. Chemical Stability of (3,1)-Chiral Graphene Nanoribbons. *ACS Nano* **2021**, *15*, 5610–5617.
- (25) Lin, Y.; Huang, Z.; Wen, X.; Rong, W.; Peng, Z.; Diao, M.; Xing, L.; Dai, J.; Zhou, X.; Wu, K. Steering Effect of Bromine on Intermolecular Dehydrogenation Coupling of Poly(p-phenylene) on Cu(111). *ACS Nano* **2020**, *14*, 17134–17141.
- (26) Zhang, C.; Hou, R.; Xu, W. Surface Organic Nanostructures Mediated by Extrinsic Components: from Assembly to Reaction. *Small Methods* **2025**, 2402118.
- (27) Zhang, Y.-Q.; Paintner, T.; Hellwig, R.; Haag, F.; Allegritti, F.; Feulner, P.; Klyatskaya, S.; Ruben, M.; Seitsonen, A. P.; Barth, J. V.; Klappenberger, F. Synthesizing Highly Regular Single-Layer Alkynyl–Silver Networks at the Micrometer Scale via Gas-Mediated Surface Reaction. *J. Am. Chem. Soc.* **2019**, *141*, 5087–5091.
- (28) Zhang, C.; Kazuma, E.; Kim, Y. Steering the Reaction Pathways of Terminal Alkynes by Introducing Oxygen Species: From C–C Coupling to C–H Activation. *J. Am. Chem. Soc.* **2022**, *144*, 10282–10290.
- (29) Zhang, C.; Jacubia, R. B.; Tanaka, Y.; Kazuma, E.; Imada, H.; Hayazawa, N.; Muranaka, A.; Uchiyama, M.; Kim, Y. Chemical Identification and Bond Control of π -Skeletons in a Coupling Reaction. *J. Am. Chem. Soc.* **2021**, *143*, 9461–9467.
- (30) Hou, R.; Gao, Y.; Guo, Y.; Zhang, C.; Xu, W. Directing Organometallic Ring–Chain Equilibrium by Electrostatic Interactions. *ACS Nano* **2024**, *18*, 31478–31484.
- (31) Ji, P.; MacLean, O.; Galeotti, G.; Dettmann, D.; Berti, G.; Sun, K.; Zhang, H.; Rosei, F.; Chi, L. Oxygen-Promoted Synthesis of Armchair Graphene Nanoribbons on Cu(111). *Sci. China: Chem.* **2021**, *64*, 636–641.
- (32) Dai, Y.; Chen, Z.; Guo, Y.; Lu, G.; Zhao, Y.; Wang, H.; Hu, P. Significant Enhancement of the Selectivity of Propylene Epoxidation for Propylene Oxide: A Molecular Oxygen Mechanism. *Phys. Chem. Chem. Phys.* **2017**, *19*, 25129–25139.

- (33) Waldmann, T.; Künzel, D.; Hoster, H. E.; Groß, A.; Behm, R. J. Oxidation of an Organic Adlayer: A Bird's Eye View. *J. Am. Chem. Soc.* **2012**, *134*, 8817–8822.
- (34) Montemore, M. M.; van Spronsen, M. A.; Madix, R. J.; Friend, C. M. O₂ Activation by Metal Surfaces: Implications for Bonding and Reactivity on Heterogeneous Catalysts. *Chem. Rev.* **2018**, *118*, 2816–2862.
- (35) Ren, J.; Wang, Y.; Zhao, J.; Tan, S.; Petek, H. K. Atom Promotion of O₂ Chemisorption on Au(111) Surface. *J. Am. Chem. Soc.* **2019**, *141*, 4438–4444.
- (36) Shi, R.; Liao, W.; Ramírez, P. J.; Orozco, I.; Mahapatra, M.; Kang, J.; Hunt, A.; Waluyo, I.; Senanayake, S. D.; Liu, P.; Rodriguez, J. A. The Interaction of K and O₂ on Au(111): Multiple Growth Modes of Potassium Oxide and Their Catalytic Activity for CO Oxidation. *Angew. Chem., Int. Ed.* **2022**, *61*, No. e202208666.
- (37) Qin, R.; Liu, K.; Wu, Q.; Zheng, N. Surface Coordination Chemistry of Atomically Dispersed Metal Catalysts. *Chem. Rev.* **2020**, *120*, 11810–11899.
- (38) Robertson, S. D.; Uzelac, M.; Mulvey, R. E. Alkali-Metal-Mediated Synergistic Effects in Polar Main Group Organometallic Chemistry. *Chem. Rev.* **2019**, *119*, 8332–8405.
- (39) Yi, Z.; Zhang, C.; Zhang, Z.; Hou, R.; Guo, Y.; Xu, W. On-Surface Synthesis of Na-Porphyrins Using NaCl as a Convenient Na Source. *Precis. Chem.* **2023**, *1*, 226–232.
- (40) Hou, R.; Guo, Y.; Yi, Z.; Zhang, Z.; Zhang, C.; Xu, W. Construction and Structural Transformation of Metal-Organic Nanostructures Induced by Alkali Metals and Alkali Metal Salts. *J. Phys. Chem. Lett.* **2023**, *14*, 3636–3642.
- (41) Liu, X.; Matej, A.; Kratky, T.; Mendieta-Moreno, J. I.; Günther, S.; Mutombo, P.; Decurtins, S.; Aschauer, U.; Repp, J.; Jelínek, P.; et al. Exploiting Cooperative Catalysis for the On-Surface Synthesis of Linear Heteroaromatic Polymers via Selective C–H Activation. *Angew. Chem., Int. Ed.* **2022**, *61*, No. e202112798.
- (42) Zhang, X.; Li, N.; Wang, H.; Yuan, C.; Gu, G.; Zhang, Y.; Nieckarz, D.; Szabelski, P.; Hou, S.; Teo, B. K.; Wang, Y. Influence of Relativistic Effects on Assembled Structures of V-Shaped Bispyridine Molecules on M(111) Surfaces Where M = Cu, Ag, Au. *ACS Nano* **2017**, *11*, 8511–8518.
- (43) Dubois, M. A.; Guillermet, O.; Gauthier, S.; Zhan, G.; Makoudi, Y.; Palmino, F.; Bouju, X.; Rochefort, A. Influence of Cu Adatoms on the Molecular Assembly of 4,4'-Bipyridine on Cu(111). *Phys. Chem. Chem. Phys.* **2018**, *20*, 15350–15357.
- (44) Yi, Z.; Guo, Y.; Hou, R.; Zhang, Z.; Gao, Y.; Zhang, C.; Xu, W. Revealing the Orientation Selectivity of Tetrapyrrolyl-Substituted Porphyrins Constrained in Molecular "Klotski Puzzles". *J. Am. Chem. Soc.* **2023**, *145*, 22366–22373.
- (45) Zhang, X.; Xue, N.; Li, C.; Li, N.; Wang, H.; Kocić, N.; Beniwal, S.; Palotás, K.; Li, R.; Xue, Q.; et al. Coordination-Controlled C–C Coupling Products via ortho-Site C–H Activation. *ACS Nano* **2019**, *13*, 1385–1393.
- (46) Huš, M.; Hellman, A. Dipole Effect on Ethylene Epoxidation: Influence of Alkali Metals and Chlorine. *J. Catal.* **2018**, *363*, 18–25.
- (47) Zhao, B.; Wang, G.-C. Theoretical Investigation of Propylene Epoxidation on Ag(111) by Molecular Oxygen: Na(K,Cl) Effects. *J. Phys. Chem. C* **2019**, *123*, 17273–17282.
- (48) Li, W.-X.; Stampfl, C.; Scheffler, M. Oxygen Adsorption on Ag(111): A Density-Functional Theory Investigation. *Phys. Rev. B* **2002**, *65*, 075407.
- (49) Scudder, P. H. *Electron Flow in Organic Chemistry: a Decision-Based Guide to Organic Mechanisms*, 2nd ed.; John Wiley & Sons, Inc.: Hoboken, NJ, 2013; p 47.
- (50) Shi, Z.; Zhang, C.; Tang, C.; Jiao, N. Recent Advances in Transition-Metal Catalyzed Reactions Using Molecular Oxygen as the Oxidant. *Chem. Soc. Rev.* **2012**, *41*, 3381–3430.
- (51) Michaelides, A.; Reuter, K.; Scheffler, M. When Seeing Is Not Believing: Oxygen on Ag(111), A Simple Adsorption System? *J. Vac. Sci. Technol., A* **2005**, *23*, 1487–1497.
- (52) Campbell, C. T. Atomic and Molecular Oxygen Adsorption on Ag(111). *Surf. Sci.* **1985**, *157*, 43–60.
- (53) Besenbacher, F. Scanning tunnelling microscopy studies of metal surfaces. *Rep. Prog. Phys.* **1996**, *59*, 1737–1802.
- (54) Laegsgaard, E.; Österlund, L.; Thstrup, P.; Rasmussen, P. B.; Stensgaard, I.; Besenbacher, F. A high-pressure scanning tunneling microscope. *Rev. Sci. Instrum.* **2001**, *72*, 3537–3542.
- (55) Kresse, G.; Hafner, J. *Ab initio* molecular dynamics for open-shell transition metals. *Phys. Rev. B* **1993**, *48*, 13115.
- (56) Kresse, G.; Furthmüller, J. Efficient iterative schemes for *ab initio* total-energy calculations using a plane-wave basis set. *Phys. Rev. B* **1996**, *54*, 11169.
- (57) Blöchl, P. E. Projector augmented-wave method. *Phys. Rev. B* **1994**, *50*, 17953.
- (58) Kresse, G.; Joubert, D. From ultrasoft pseudopotentials to the projector augmented-wave method. *Phys. Rev. B* **1999**, *59*, 1758.
- (59) Perdew, J. P.; Burke, K.; Ernzerhof, M. Generalized gradient approximation made simple. *Phys. Rev. Lett.* **1996**, *77*, 3865.
- (60) Grimme, S.; Antony, J.; Ehrlich, S.; Krieg, H. A consistent and accurate *ab initio* parametrization of density functional dispersion correction (DFT-D) for the 94 elements H–Pu. *J. Chem. Phys.* **2010**, *132*, 154104.
- (61) Tersoff, J.; Hamann, D. R. Theory of the scanning tunneling microscope. *Phys. Rev. B* **1985**, *31*, 805.
- (62) Nosé, S. A unified formulation of the constant temperature molecular dynamics methods. *J. Chem. Phys.* **1984**, *81*, 511–519.
- (63) Nosé, S. Constant temperature molecular dynamics methods. *Prog. Theor. Phys. Suppl.* **1991**, *103*, 1–46.
- (64) Hoover, W. G. Canonical dynamics: Equilibrium phase-space distributions. *Phys. Rev. A* **1985**, *31*, 1695.
- (65) Henkelman, G.; Uberuaga, B. P.; Jónsson, H. A climbing image nudged elastic band method for finding saddle points and minimum energy paths. *J. Chem. Phys.* **2000**, *113*, 9901–9904.